Tuning of electronic and optical properties of a predicted silicon allotrope: Hexagonal silicon h10-Si

Deju Zhang [1], Haiyang Niu,[2] Yunguo Li [3,4] Hong-Mei Huang,[1] Peng Jiang [1,*] and Yan-Ling Li [1,†]

[1]*School of Physics and Electronic Engineering, Jiangsu Normal University, Xuzhou 221116, China*

[2]*State Key Laboratory of Solidification Processing, International Center for Materials Discovery, School of Materials Science and Engineering, Northwestern Polytechnical University, Xi'an 710072, China*

[3]*CAS Key Laboratory of Crust-Mantle Materials and Environments, School of Earth and Space Sciences, University of Science and Technology of China, Hefei 230026, China*

[4]*CAS Center for Excellence in Comparative Planetology, University of Science and Technology of China, Hefei 230026, China*

The indirect band gap of the diamondlike silicon does not allow direct travel of electrons between valence band and conduction band edges, which has limited its application and performance in optoelectronic devices. Searching new silicon allotropes with highly tunable or direct band gap becomes more and more urgent with the increasing demand on clean energy. Here, we predict a silicon allotrope, h10-Si, which is an indirect-gap semiconductor with a band gap of about 0.96 eV. Furthermore, the electronic and optical properties exhibit a strong dependence on strain. In particular, the indirect band gap of the predicted silicon allotrope can be switched to a direct band gap at a uniaxial tensile strain of about 8% and the light absorption can be tuned continuously in a wide range of photon energy. Besides, the single-layer counterpart of this allotrope is confirmed to be dynamically stable and more stable in energy than silicene, endowing it with potential applications in nanoscale devices.

I. INTRODUCTION

Silicon with the cubic diamond structure (d-Si) under ambient conditions has been widely used in the electronic and optoelectronic industries for more than half a century [1]. However, the intrinsic characteristic of the indirect band gap of d-Si limits its light emission and absorption efficiency [2,3]. In order to overcome the limitation of d-Si one can resort to either property tailoring or new material designing. In the past decades, great effort has been dedicated to customizing the band structure of d-Si using various techniques, such as impurity, defect, and interface manipulations [4–6], as well as pressure and strain engineerings [7,8]. Among them, strain engineering, as a perfect method, has been widely used in theory and experiment to modify physical properties of materials, such as magnetism [9], band structure [10], optical property [11,12], and superconductivity [13,14]. For silicon-based materials, it has been proved that the electron and hole mobilities can be significantly enhanced by interfacial strains caused by the substrate [15,16]. Homewood *et al.* found that impurity-induced strain can change the energy band structure of silicon [17]. It has also been reported that, under biaxial tensile strain, the optical band gap of silicon decreases significantly, creating excellent photosensitivity in silicon nanofilm photodetectors [18].

On the other hand, low-energy silicon allotropes or silicon-based alloys with improved electronic and optical properties are promising substitutes for d-Si. Various metallic silicon allotropes, such as Si-II, can form under high pressures [19]. Upon pressure release, Si-II would transform to other metastable allotropes with distorted tetrahedral framework. Body-centered BC8 belongs to this case. Hexagonal diamond Si, produced by heating BC8 above 470 K, possesses an indirect band gap of about 1 eV [20,21]. However, none of the above allotropes show satisfying or tunable electronic and optical properties. This situation naturally requires high-throughput searching for more silicon allotropes with attractive electronic and optical properties by means of the crystal structure prediction methods [22–24]. 11 metastable silicon allotropes exhibiting intriguing electronic properties with either direct or quasidirect band gap in the range of 1.0–1.8 eV were proposed by using a modified *ab initio* minima hopping crystal structural prediction method [22]. More direct or quasidirect band gap silicon allotropes have also been found by using various other algorithms [23,24]. Although the emerging silicon allotropes show the promising electronic and optical properties, it remains a question how to realize them experimentally. Besides, it is unclear but interesting to see how their electronic and optical properties evolve under different physical and chemical settings.

In this paper, state-of-the-art first-principles calculations combined with evolutionary algorithm are used to predict a silicon allotrope denoted as h10-Si, which can be obtained by removing guest potassium atoms from a candidate precursor $P6/mmm$-KSi$_{10}$. First, we demonstrate the thermal, dynamical, and mechanical stabilities of h10-Si. Then, we show that h10-Si is a semiconductor with an indirect band gap of about 0.96 eV, and it has tunable electronic and optical properties.

*pjiang@jsnu.edu.cn
†ylli@jsnu.edu.cn

The application of the uniaxial compressive strain leads to the narrowing of band gap of h10-Si, while the band gap first increases smoothly and then decreases with the increasing tensile strain. Especially, a tensile strain of 8% can trigger the indirect-to-direct band gap transition. More interestingly, the single-layer h10-Si is not only dynamically stable but more stable in energy than the reported silicene [25]. Thus the single-layer h10-Si is expected to be synthesized experimentally. Overall, this study provides a route for designing and synthesizing silicon allotropes and two-dimensional silicenes.

II. METHODS

The low-energy structures were searched via the evolutionary algorithm as implemented in the USPEX code [26,27], and the underlying *ab initio* structural relaxations were carried out within the framework of density functional theory (DFT) as implemented in the Vienna *ab initio* simulation package (VASP) [28,29]. The generalized gradient approximation (GGA) with the Perdew-Burke-Ernzerhof (PBE) functional and projector augmented wave (PAW) potentials were used [30–32]. The electronic configurations $2s^2 2p^2$ were treated as valence electrons for Si atoms. For the crystal structure search, we used a plane-wave basis set cutoff of 400 eV and performed the Brillouin zone (BZ) integrations using a coarse k-point grid. The low-energy structures were further relaxed at a higher level of accuracy with a k-point grid of spacing $2\pi \times 0.018$ Å^{-1}. Iterative relaxation of atomic positions was stopped until the force on each atom is less than 0.001 eV Å^{-1} and the energy convergence criteria of 1×10^{-5} eV are met. The molecular dynamics (MD) simulations were performed using the canonical *NVT* and *NPT* ensembles up to 800 K. A $2 \times 2 \times 4$ supercell containing 160 Si atoms was adopted. The phonon spectra were calculated by using the PHONOPY code based on the finite displacement method [33], in which a $2 \times 2 \times 1$ supercell and a Monkhorst-Pack k-point mesh of $2 \times 2 \times 3$ were used. The Heyd-Scuseria-Ernzerhof version functional (HSE06) [34] was also used for electronic structure calculations. The dielectric functions were calculated by using a quasiparticle method combined with the Bethe-Salpeter equation (G$_0$W$_0$+BSE) [35,36], in which we used a plane-wave basis set cutoff of 400 eV (200 eV for response function) and performed the BZ integrations using a Monkhorst-Pack k-point grid of $4 \times 4 \times 4$.

III. RESULTS AND DISCUSSION

A. Structure and stability

In the theoretical design of group IV-A element allotropes, we have previously proposed an indirect search scheme to design a carbon allotrope with the open-channel feature by removing calcium atoms from a carbon-rich precursor [37–39]. This methodology has been successfully applied to design and synthesize $Cmcm$-Si$_{24}$ [3], and this idea is also called the "two-step" method. In this method, the key is to find a suitable precursor [40–42]. Here, we systematically searched the alkali-metal and alkaline-earth-metal (M) silicides with various composition ratios, M$_x$Si$_y$ (x:$y = 1:2$, $1:4$, $1:6$, $1:8$, $1:10$, $1:12$), via the *ab initio* evolutionary algorithm. Finally, we found six dynamically stable low-energy precur-
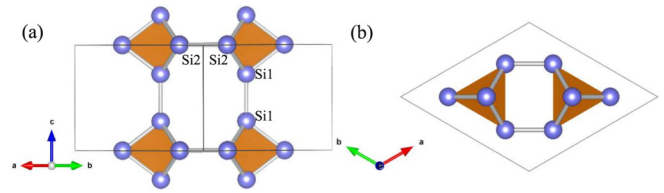

FIG. 1. (a) Side and (b) top views of h10-Si. The Si atoms are connected to form 8-Si and 6-Si channels and the two kinds of channels are perpendicularly connected by hexahedral building blocks. The building blocks are represented by orange polyhedrons and two inequivalent Si atoms are labeled by Si1 and Si2, respectively

sors with the open-channel feature and their crystal structure, phonon spectra, and lattice parameters are shown in Figs. S1 and S2 and Table S1 of the Supplemental Material (SM) [43]. Among these, $Fmmm$-Sr$_4$Si$_{24}$ and $Fmmm$-Ca$_4$Si$_{24}$ have the same structural framework. Therefore, five silicon allotropes were obtained. Four of them ($Cmcm$-Si$_{24}$ [3], $Fddd$-Si$_{48}$ [22], $Fmmm$-Si$_{24}$ [44], and $Im\bar{3}m$-Si$_6$ [45]) are readdressed ones and the remaining one has not been reported yet. Note that, in the previous works [22,44], the researchers predicted the structures of silicon allotropes, but the pathway to synthesize them was not mentioned. Therefore, our findings suggest an effective route or reference for the experimental synthesis of silicon allotropes. More details and results can be found in the SM [43]. As shown in Fig. 1, the silicon allotrope crystallized in a hexagonal structure ($P6/mmm$, No. 191). In this structure, ten Si atoms lie in two inequivalent Wyckoff $4h$ and $6l$ sites. According to the symmetry of the structure and the number of Si atoms in the primitive cell, the silicon allotrope is referred to as h10-Si. Structurally, the Si atoms are connected to form 8-Si and 6-Si channels, and the two kinds of channels are perpendicularly connected by the hexahedral building block (see Fig. 1). Interestingly, this channel feature in h10-Si is similar to that in $Cmcm$-Si$_{24}$ synthesized experimentally by the two-step synthesis methodology [3]. As such there is an expectation that h10-Si can also be synthesized by removing potassium atoms from a candidate precursor $P6/mmm$-KSi$_{10}$ (see Fig. S2 in the SM [43]). For h10-Si, the equilibrium volume (V_0) and bulk modulus (B_0) are obtained by fitting the total energy at different volumes to the third-order Birch-Murnaghan equation of states (EOS) [46]. The optimized equilibrium structural parameters V_0, B_0 and density are 246.22 Å^3, 72 GPa, and 1.893 g/cm^3, respectively. The equilibrium lattice parameters of h10-Si are $a = b = 7.3643$ Å and $c = 5.2422$ Å, and the Wyckoff sites of two inequivalent Si atoms are $4h$ (1/3, 2/3, 0.7247) and $6l$ (0.1852, 0.8148, 0.0), respectively. Meanwhile, to evaluate the relative energetic stability between different silicon allotropes, the calculated energy-volume curves of h10-Si and d-Si, along with the reported silicon allotropes $Cmcm$-Si$_{24}$ [3], mC12-Si, tI16-Si, tP16-Si [23], and $P6/m$-Si$_6$ [47], are plotted in Fig. 2(a). It is clearly shown that our proposed h10-Si is highly competitive in energy compared to the selected allotropes reported so far. The energy of h10-Si is 0.04 eV/atom and 0.12 eV/atom lower than those of tP16-Si and $P6/m$-Si$_6$, respectively [23,47], and slightly higher than those of d-Si, mC12-Si, $Cmcm$-Si$_{24}$, and tI16-Si. Considering
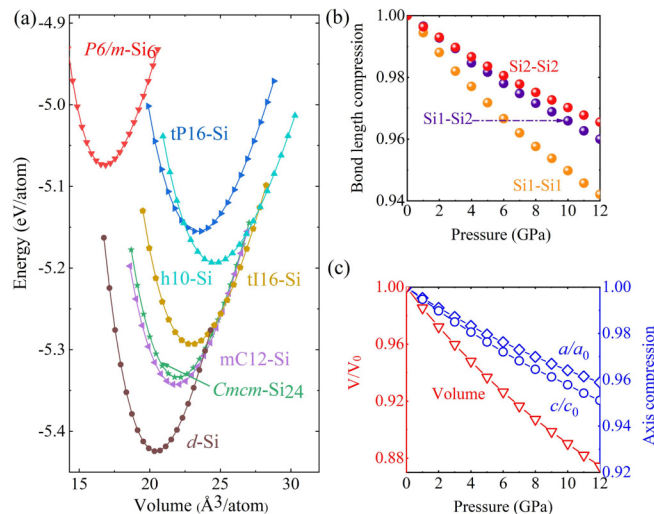
FIG. 2. (a) Energy-volume curves of $h10$-Si and other siliconallotropes. (b) Fractional bond length compression as a function of pressure. (c) V/V_0 and fractional axis compression as a functions of pressure. V_0 is the equilibrium volume and a_0 as well as c_0 are the corresponding equilibrium lattice parameters.

that high temperature can lead to material decomposition, we further explore the thermal stability of $h10$-Si. The *NVT* and *NPT*-MD simulations are performed at finite temperatures and the results are shown in Fig. S3 of the SM [43]. Obviously, there is no tendency of decomposition up to 800 K in $h10$-Si, indicating that the thermal stability of $h10$-Si is better than that of $P6/m$-Si$_6$ with the critical temperature of 400 K [47]. This can be easily understood as the rigid hexahedral building block can stabilize the crystal structure of $h10$-Si when the external environment is deteriorated.

It is essential to examine dynamical and mechanical stabilities of the predicted $h10$-Si by means of phonon spectrum and elastic constants. The calculated phonon spectra at ambient pressure are shown in Fig. S4 of the SM [43]. The absence of the imaginary frequency throughout the BZ signals its dynamical stability. The calculated elastic constants are $C_{11} = 147$ GPa, $C_{12} = 42$ GPa, $C_{13} = 19$ GPa, $C_{33} = 149$ GPa, $C_{44} = 10$ GPa, and $C_{66} = 53$ GPa, respectively. The values satisfy the mechanical stability criteria for the hexagonal system [48], namely, $C_{11} > |C_{12}|$, $2C_{13}^2 < C_{33}(C_{11} + C_{12})$, $C_{44} > 0$, and $C_{66} > 0$, indicating that $h10$-Si is mechanically stable. From the full elastic constant tensor, we can determine the bulk modulus B_0 according to the Voigt-Reuss-Hill (VRH) approximation [49]. The obtained value of B_0 is about 67 GPa, which agrees well with that by fitting EOS. In addition, we explored the effects of pressure on the bond lengths and lattice parameters. As shown in Fig. 2(b), the change in the lengths of Si1-Si2 and Si2-Si2 bonds is obviously lower than that of the Si1-Si1 bond, thus making the c axis direction have good compressibility. This could be well understood by means of the calculated fractional axis compression as the functions of pressure [see Fig. 2(c)]. From Fig. 2(c), one can see that the compressibility along c axis direction is higher than that of a axis or b axis direction. The additional calculation shows that the deformation along c axis direction is mainly contributed
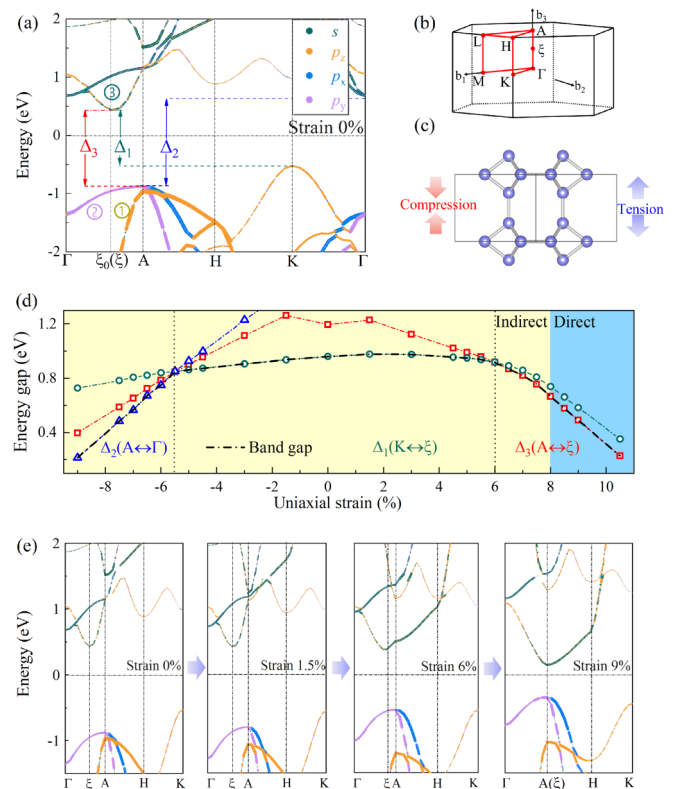

FIG. 3. (a) Band structure of pristine $h10$-Si. Several bands significantly affected by uniaxial strain are numbered as band 1, band 2, and band 3 and the individual energy gaps are represented by arrow lines. (b) Brillouin zone (BZ) and the high-symmetry k points. (c) Schematic diagram of uniaxial compressive and tensile strains. (d) Individual energy gaps of $h10$-Si under different strains. Δ_1, Δ_2, Δ_3 denote the energy differences between the CBM at ξ, Γ, ξ points and the VBM at K, A, A points, namely, $(K \leftrightarrow \xi)$, $(A \leftrightarrow \Gamma)$, $(A \leftrightarrow \xi)$, respectively. The dotted line denotes the band gap. (e) The band structures evolution under the uniaxial strains of 0%, 1.5%, 6%, and 9%.

by the Si1-Si1 bond under pressure (see Fig. S5 in the SM [43]).

B. Electronic properties

Since all valence electrons are strictly constrained in the sp^3 hybrid orbitals, pristine $h10$-Si is an indirect-gap semiconductor with a band gap of 0.42 eV at the PBE level. It is well known that the PBE functional generally underestimates the band gap of the conventional bulk semiconductors, so we performed calculations with the hybrid functional HSE06 to correct this band gap. As shown in Fig. 3(a), the calculated HSE06 band structure can confirm the indirect-gap feature of $h10$-Si and the calculated band gap at HSE06 level is about 0.96 eV, where the valence band maximum (VBM) and conduction band minimum (CBM) are located at the A (0.0, 0.0, 0.5) and ξ_0 (0.0, 0.0, 0.316) points. Here, the ξ_0 point is defined as the k point with the CBM in pristine $h10$-Si, and the high-symmetry points in BZ are shown in Fig. 3(b). In addition, we have performed the band structure calculation of pristine $h10$-Si by adopting the quasiparticle G_0W_0 method

(see Fig. S6 in the SM [43]). The calculated G_0W_0 band gap is about 0.78 eV, which is slightly smaller than that from HSE06. But the qualitative features of the bands remain the same. All methods clearly suggest the indirect-gap characteristic of pristine h10-Si. From the analysis of the orbital projected band structure shown in Fig. 3(a), it is found that the top valence band (band 1) originates mostly from p_z orbitals and second top valence bands (band 2) attribute mainly to p_x and p_y orbitals, while the CBM are mainly from s/p_z hybrid orbitals.

The energy band structure of a conventional semiconductor is usually sensitive to external pressure or volume deformation [50,51]. Since h10-Si is easily compressed along the c axis direction, it is highly expected that some interesting electronic properties of h10-Si can be revealed by applying a uniaxial strain along c direction shown in Fig. 3(c). Figure S7 in the SM shows the band structures of h10-Si at different values of uniaxial strains [43]; we found that the strain has a remarkable effect on the band structure along two particular k directions in BZ, namely, Γ to A and A to H. Interestingly, the changes of band structures exhibit a strong dependence on the applied strain. For the negative or compressive strain, the band gap is first decreased gently with the increasing strain and then narrowed sharply at a critical strain value of -5.5% [see Fig. 3(d)]. We need to point out that, with the compressive strain smaller than 5.5%, the band gap is still Δ_1 (the energy differences between the CBM at ξ point and the VBM at K point) shown in Figs. 3(a) and 3(d) and Fig. S7 of the SM [43]. The particular phenomenon of the sharp change in the band gap is because, with the compressive strain larger than 5.5%, the conduction band at Γ point has a lower energy than that at ξ point and the valence band at A point has a higher energy than that at K point. Thus CBM moves to Γ point and VBM moves to A point, that is, the band gap becomes Δ_2 (the energy difference between the CBM at Γ point and the VBM at A point), as shown in Figs. 3(a) and 3(d) and Fig. S7 of the SM [43]. This leads to a great change of the band gap in slope. For positive or tensile strain, the band gap increases marginally with the strain smaller than about 1.5% and further reduces smoothly until the strain is smaller than 6%, and finally decreases quickly with the strain larger than 6%. Note that the band gap is Δ_1 when the tensile strain is smaller than 6%. The sudden change of the band gap at a critical strain of 6% is a result of the change of the location of VBM from K to A point; the band gap becomes Δ_3 (the energy difference between the CBM at ξ point and the VBM at A point), which can be clearly observed in Figs. 3(a), 3(d) and 3(e). Very interestingly, the uniaxial tensile strain with a value in excess of about 8% also causes an indirect-to-direct band gap transition. Moreover, we also checked the band structures of h10-Si by G_0W_0 calculation at different tensile strains (see Fig. S6 in the SM [43]). The G_0W_0 critical tensile strain is about 9% for the indirect-to-direct band gap transition, which is slightly larger than that calculated by HSE06. However, the overall trending of the strain-dependent band evolution from both methods is the same, demonstrating the accuracy of our results. It has been experimentally demonstrated that the extreme uniaxial compressive and tensile strains can be achieved up to -19% and 12%, respectively [52,53]. Note that the range of strain applied in our predicted h10-Si is still in the reach of experimental facility. In addition, the dynamical

stability of h10-Si is still maintained within a wide strain range from -9.0% to 10.5% (see Fig. S8 in the SM [43]). Therefore, once h10-Si is successfully experimentally synthesized, the indirect-to-direct band gap transition by strain engineering is highly possible.

To better understand the physical mechanism behind the indirect-to-direct band gap transition, we tracked the evolution of the band structures at the uniaxial tensile strains of 0%, 1.5%, 6%, and 9% shown in Fig. 3(e). We found that, compared with band 1 contributed by p_z orbitals, band 2 contributed by p_x and p_y orbitals moves toward the Fermi level with the increasing strain, resulting in A point becoming a VBM beyond a strain of 6%. This is due to the fact that the application of the uniaxial tensile strain can weaken the interactions between p_z orbitals at the same time the p_x and p_y orbitals in the a-b plane are mildly enhanced [10]. The enhanced interactions of p_x and p_y orbitals can further strengthen Coulomb repulsion, which results in the energy level of band 2 shifting up. On the other hand, with the downward shift in energy of band 3, the CBM can continuously move toward A point with the increasing tensile strain. To describe this behavior, we define the location of the CBM as ξ point (ξ is a dynamic point with the change of the tensile strain). The downward shift of band 3 is because the hybridization between s and p_z orbitals is strengthened with the increasing strain, according to the strain dependent partial density of states (PDOS) (see Fig. S9 in the SM [43]), which pulls down the energy of the maximum unoccupied s orbital around A point [54]. Furthermore, to understand the evolution of the CBM, we calculated the characteristic charge density for band 3 at ξ_0 and A points with 0% and 9% strains. As shown in Figs. 4(a) and 4(b), the occupation of p orbitals increases with the strain. In detail, the enhancement of the hybridization between s and p_z is stronger at A point than that at ξ_0 point, which leads to a relatively quick downward shift of band 3 in energy at A point. Therefore, A point becomes the location of CBM with tensile strain higher than 8%. Besides, the VBM is still located at A point with the tensile strain larger than 6%; thus an indirect-direct gap transition occurs at the critical tensile strain of 8%. Usually, one can achieve the indirect-to-direct band gap transition by spatially melding direct- or indirect-gap germanium in silicon crystal [1,55]. In comparison, strain-induced indirect-to-direct band gap transition of h10-Si shows unparalleled advantage of reversibility and purity, which is important for silicon-based green information and communication technologies.

C. Optical properties

The optical property of a semiconductor is directly related to its electronic structure. In view of the electronic structure of h10-Si exhibiting a strong dependence on strain, one can conclude that the optical properties of h10-Si can be effectively tuned by applying strain. We investigated the optical absorption spectrum (ε_2) of h10-Si with and without uniaxial strains by using the BSE+G_0W_0 method (see Fig. 5). The theoretical and experimental ε_2 of d-Si combined with the reference air mass (AM) 1.5 solar spectral irradiance are also considered for comparison [56,57]. As shown in Fig. 5(a), there are two absorption peaks located at 2.46 eV (the low-energy peak)
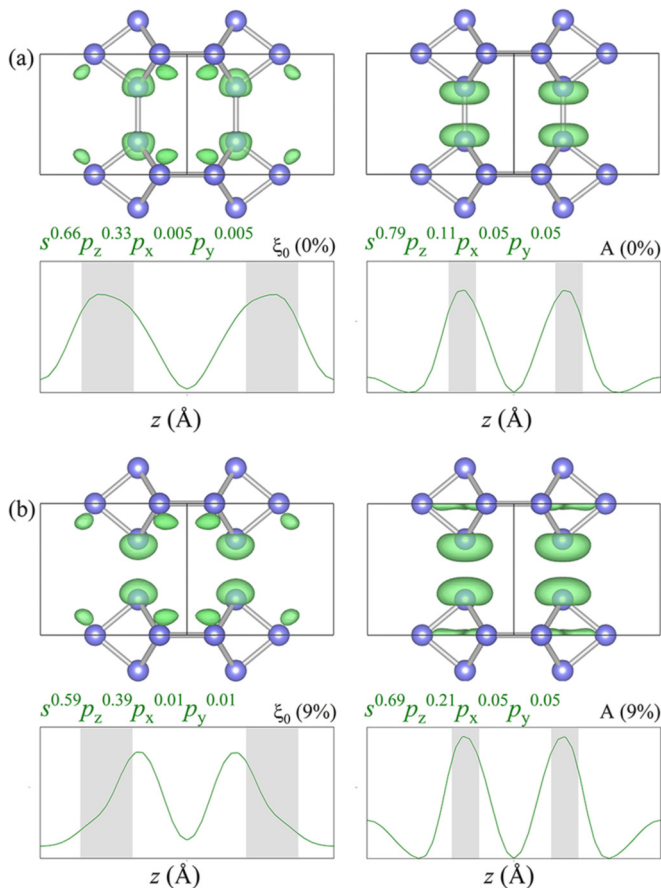
FIG. 4. Characteristic charge density and the corresponding planar average along c axis (z) direction at ξ_0 and A points under (a) 0% and (b) 9% strains, respectively. The orbital compositions are written as superscripts.

FIG. 5. (a) Optical absorption spectrum (ε_2) of pristine h10-Si without any uniaxial strains as a function of the photon energy with respect to that of d-Si and solar spectral irradiance. (b) The continuous shift of the low-energy peak with a wide range of strains from -3% to 7.5%. The chromatic bars on top of spectra indicate the regions of infrared (IR), visible (VIS), and ultraviolet (UV) light.

and 2.88 eV (the high-energy peak) in the visible (VIS) light range, respectively. This means that, compared with d-Si, the light absorption of pristine h10-Si is significantly higher below 3.3 eV, particularly in the visible light range where solar spectral irradiation has its maximum intensity. Figure 5(b) displays the optical absorption spectrum of h10-Si at different strains. Similar to the electronic properties, the optical absorption also exhibits a strong strain dependence. While the low-energy peak is moved up to 2.76 eV at a uniaxial compressive strain of -3%, it moved down to 1.56 eV with a tensile strain of 7.5%. By comparison, the magnitude of the total shift is larger than that in Si-Ge alloy and comparable to that in black phosphorus [1,58].

The important role of strain has been extensively exploited to tune the optoelectronic properties. For examples, the application of the tensile strain is found to improve emission in bulk germanium [59] and drive the indirect-to-direct optical transition in two-dimensional bilayer WSe$_2$ [60,61]. Not surprisingly, the strain induced absorption improvement in h10-Si may facilitate its application in optoelectronic devices.

D. Single-layer h10-Si

In the past two decades, interest in graphene has grown rapidly. Naturally one should question whether the other
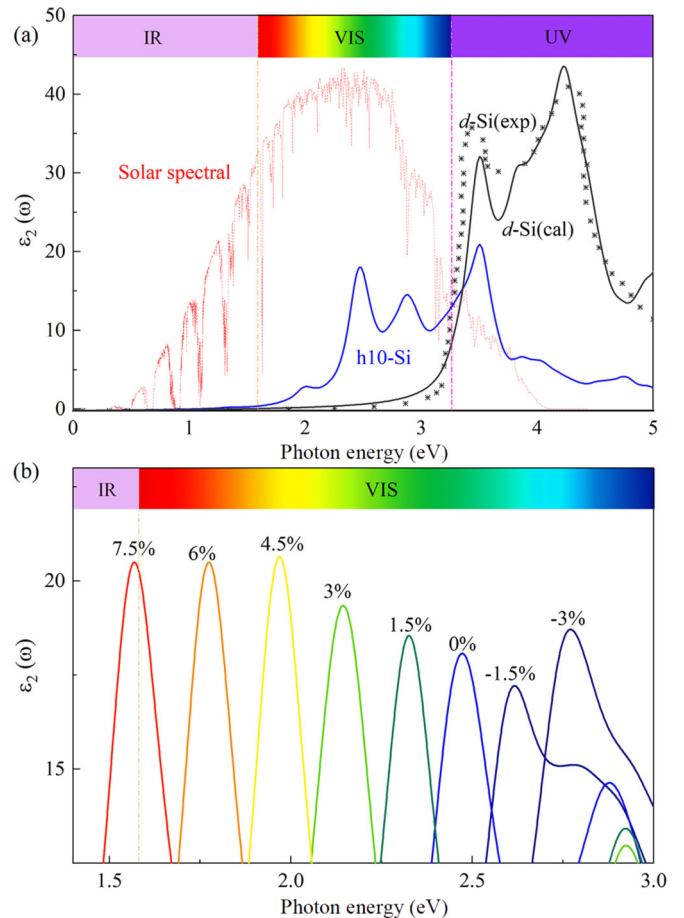
group IV-A elements in the Periodic Table have a stable two-dimensional (2D) structure [62,63]. Experimentally, through surface segregation on zirconium diboride thin films grown on Si wafers, a 2D epitaxial silicene was obtained [64]. In addition, several silicene allotropes with various buckled parameters were successfully epitaxially grown on silver (111) substrate [65–67]. Interestingly, due to the robust structural stability of the hexahedral building block, the single-layer counterpart of h10-Si is expected to be stable under ambient conditions. To estimate the energetic stability of the single-layer h10-Si, we calculated its total energy. It shows that the total energy of single-layer h10-Si is about 0.22 eV/atom lower than that of silicene [25], implying that the single-layer h10-Si is highly accessible experimentally. In addition, it is found that the single-layer h10-Si is an indirect-gap semiconductor with a band gap of about 0.67 eV at the HSE06 level. Moreover, the calculated phonon spectra can confirm the dynamical stability of the single-layer h10-Si at ambient pressure, as shown in Fig. S10 in the SM [43]. We also note that this particular single-layer structure has been briefly discussed in the theoretical work [68]. The finding of single-layer h10-Si provides not only a paradigm for understanding the

energy landscape of silicene allotropes, but also an evidence for the existence of a stable single-layer counterpart in covalent bulk silicon systems.

IV. CONCLUSION

In conclusion, we have predicted a silicon allotrope, h10-Si, exhibiting an indirect-gap semiconducting characteristic with a band gap of about 0.96 eV. Its thermal, dynamical, and mechanical stabilities have been verified by MD simulations, and the calculated phonon spectra as well as elastic constants. It is found that the band gap of h10-Si can be continuously tuned by the uniaxial strains along c axis direction. More interestingly, h10-Si may occur as an indirect-to-direct band gap transition beyond a uniaxial tensile strain of 8% at the HSE06 level, which is attributed to the change of the orbital hybridization. In addition, the continuous blueshift or redshift

can be induced by the strain, which may have a potential application in the optoelectronic devices. Furthermore, we have predicted a low-energy single-layer h10-Si that is highly expected to be achievable experimentally. Our findings not only provide a paradigm for understanding strain engineering in a pure silicon system but also open up a route to fabricate and design group IV-A element allotropes with the polyhedral building block.

[1] E. M. Fadaly, A. Dijkstra, J. R. Suckert, D. Ziss, M. A. van Tilburg, C. Mao, Y. Ren, V. T. van Lange, K. Korzun, S. Kölling *et al.*, Nature (London) **580**, 205 (2020).

[2] Z. Zhao, F. Tian, X. Dong, Q. Li, Q. Wang, H. Wang, X. Zhong, B. Xu, D. Yu, J. He *et al.*, J. Am. Chem. Soc. **134**, 12362 (2012).

[3] D. Y. Kim, S. Stefanoski, O. O. Kurakevych, and T. A. Strobel, Nat. Mater. **14**, 169 (2015).

[4] M. Wang, A. Debernardi, Y. Berencén, R. Heller, C. Xu, Y. Yuan, Y. Xie, R. Böttger, L. Rebohle, W. Skorupa *et al.*, Phys. Rev. Appl. **11**, 054039 (2019).

[5] X. Chen, L. Li, J. Zhang, Y. Jian, G. Yang, X. Liu, G. Zeng, Y. Pang, X. Yu, X. Meng *et al.*, J. Phys. D: Appl. Phys. **54**, 265103 (2021).

[6] P. Xiaowen Fang, S. Nihtianov, P. Sberna, and C. Fang, Phys. Rev. B **103**, 075301 (2021).

[7] J. Z. Hu, L. D. Merkle, C. S. Menoni, and I. L. Spain, Phys. Rev. B **34**, 4679 (1986).

[8] H. Omi, D. J. Bottomley, Y. Homma, and T. Ogino, Phys. Rev. B **67**, 115302 (2003).

[9] D. Kumar, A. David, A. Fouchet, A. Pautrat, J. Varignon, C. U. Jung, U. Lüders, B. Domengès, O. Copie, P. Ghosez, and W. Prellier, Phys. Rev. B **99**, 224405 (2019).

[10] B. Ram and A. K. Singh, Phys. Rev. B **95**, 075134 (2017).

[11] G. C. Osbourn, Phys. Rev. B **27**, 5126 (1983).

[12] A. Adams, Electron. Lett. **22**, 249 (1986).

[13] C. Liu, X. Song, Q. Li, Y. Ma, and C. Chen, Phys. Rev. Lett. **124**, 147001 (2020).

[14] J. P. Ruf, H. Paik, N. J. Schreiber, H. P. Nair, L. Miao, J. K. Kawasaki, J. N. Nelson, B. D. Faeth, Y. Lee, B. H. Goodge *et al.*, Nat. Commun. **12**, 59 (2021).

[15] J. Welser, J. Hoyt, and J. Gibbons, IEEE Electron Device Lett. **15**, 100 (1994).

[16] L. Washington, F. Nouri, S. Thirupapuliyur, G. Eneman, P. Verheyen, V. Moroz, L. Smith, X. Xu, M. Kawaguchi, T. Huang, K. Ahmed, M. Balseanu, L.-Q. Xia, M. Shen, Y. Kim, R. Rooyackers, K. D. Meyer, and R. Schreutelkamp, IEEE Electron Device Lett. **27**, 511 (2006).

[17] W. L. Ng, M. Lourenco, R. Gwilliam, S. Ledain, G. Shao, and K. Homewood, Nature (London) **410**, 192 (2001).

[18] A. K. Katiyar, K. Y. Thai, W. S. Yun, J. Lee, and J.-H. Ahn, Sci. Adv. **6**, eabb0576 (2020).

[19] J. C. Jamieson, Science **139**, 762 (1963).

[20] B. D. Malone, J. D. Sau, and M. L. Cohen, Phys. Rev. B **78**, 035210 (2008).

[21] J. M. Besson, E. H. Mokhtari, J. Gonzalez, and G. Weill, Phys. Rev. Lett. **59**, 473 (1987).

[22] M. Amsler, S. Botti, M. A. L. Marques, T. J. Lenosky, and S. Goedecker, Phys. Rev. B **92**, 014101 (2015).

[23] Q. Wang, B. Xu, J. Sun, H. Liu, Z. Zhao, D. Yu, C. Fan, and J. He, J. Am. Chem. Soc. **136**, 9826 (2014).

[24] C. He, X. Shi, S. J. Clark, J. Li, C. J. Pickard, T. Ouyang, C. Zhang, C. Tang, and J. Zhong, Phys. Rev. Lett. **121**, 175701 (2018).

[25] C.-L. Lin, R. Arafune, K. Kawahara, N. Tsukahara, E. Minamitani, Y. Kim, N. Takagi, and M. Kawai, Appl. Phys. Express **5**, 045802 (2012).

[26] A. O. Lyakhov, A. R. Oganov, H. T. Stokes, and Q. Zhu, Comput. Phys. Commun. **184**, 1172 (2013).

[27] C. W. Glass, A. R. Oganov, and N. Hansen, Comput. Phys. Commun. **175**, 713 (2006).

[28] J. Hafner, Comput. Phys. Commun. **177**, 6 (2007).

[29] G. Kresse and J. Furthmüller, Phys. Rev. B **54**, 11169 (1996).

[30] N. Holzwarth, A. Tackett, and G. Matthews, Comput. Phys. Commun. **135**, 329 (2001).

[31] J. P. Perdew, K. Burke, and M. Ernzerhof, Phys. Rev. Lett. **77**, 3865 (1996).

[32] K. Parlinski, Z. Q. Li, and Y. Kawazoe, Phys. Rev. Lett. **78**, 4063 (1997).

[33] S. Baroni, S. De Gironcoli, A. Dal Corso, and P. Giannozzi, Rev. Mod. Phys. **73**, 515 (2001).

[34] J. Heyd, G. E. Scuseria, and M. Ernzerhof, J. Chem. Phys. **118**, 8207 (2003).

[35] E. E. Salpeter and H. A. Bethe, Phys. Rev. **84**, 1232 (1951).

[36] L. X. Benedict and E. L. Shirley, Phys. Rev. B **59**, 5441 (1999).

[37] Y.-L. Li, W. Luo, X.-J. Chen, Z. Zeng, H.-Q. Lin, and R. Ahuja, Sci. Rep. **3**, 3331 (2013).

[38] X. Jiang, J. Zhao, Y.-L. Li, and R. Ahuja, Adv. Funct. Mater. **23**, 5846 (2013).

[39] Y.-L. Li, S.-N. Wang, A. R. Oganov, H. Gou, J. S. Smith, and T. A. Strobel, Nat. Commun. **6**, 6974 (2015).

[40] J. Wu, H. Gao, K. Xia, D. Xing, and J. Sun, Appl. Phys. Lett. **111**, 173904 (2017).

[41] C.-M. Hao, Y. Li, H.-M. Huang, and Y.-L. Li, J. Chem. Phys. **148**, 204706 (2018).

[42] S. Ding, J. Shi, J. Xie, W. Cui, P. Zhang, K. Yang, J. Hao, L, Zhang, and Y. Li, npj Comput. Mater. **7**, 89 (2021).

[43] See Supplemental Material at http://link.aps.org/supplemental/10.1103/PhysRevB.104.125201 for the computational details and results of the structure prediction; Phonon spectra and AIMD simulations of the pristine h10-Si; Pressure dependence of the individual distances of h10-Si; Electronic band evolutions of h10-Si at the G_0W_0 and HSE06 levels; Phonon spectra and partial density of states of h10-Si at different strains; Band structure and phonon spectra of the single-layer h10-Si.

[44] A. Marzouk, P. B. Balbuena, and F. El-Mellouhi, Electrochim. Acta **207**, 301 (2016).

[45] A. Jain, S. P. Ong, G. Hautier, W. Chen, W. D. Richards, S. Dacek, S. Cholia, D. Gunter, D. Skinner, G. Ceder *et al.*, APL Mater. **1**, 011002 (2013).

[46] F. Birch, Phys. Rev. **71**, 809 (1947).

[47] H.-J. Sung, W. H. Han, I.-H. Lee, and K. J. Chang, Phys. Rev. Lett. **120**, 157001 (2018).

[48] F. Mouhat and F.-X. Coudert, Phys. Rev. B **90**, 224104 (2014).

[49] R. Hill, Proc. Phys. Soc. A **65**, 349 (1952).

[50] W.-J. Yin, S. Chen, J.-H. Yang, X.-G. Gong, Y. Yan, and S.-H. Wei, Appl. Phys. Lett. **96**, 221901 (2010).

[51] S.-H. Wei and A. Zunger, Phys. Rev. B **60**, 5404 (1999).

[52] J. M. Wheeler, R. Raghavan, J. Wehrs, Y. Zhang, R. Erni, and J. Michler, Nano Lett. **16**, 812 (2016).

[53] M.-F. Yu, O. Lourie, M. J. Dyer, K. Moloni, T. F. Kelly, and R. S. Ruoff, Science **287**, 637 (2000).

[54] L.-D. Yuan, H.-X. Deng, S.-S. Li, S.-H. Wei, and J.-W. Luo, Phys. Rev. B **98**, 245203 (2018).

[55] M. d'Avezac, J.-W. Luo, T. Chanier, and A. Zunger, Phys. Rev. Lett. **108**, 027401 (2012).

[56] H. Philipp and H. Ehrenreich, Phys. Rev. **129**, 1550 (1963).

[57] P. Nozieres and D. Pines, Phys. Rev. **113**, 1254 (1959).

[58] D. Çakır, H. Sahin, and F. M. Peeters, Phys. Rev. B **90**, 205421 (2014).

[59] M. El Kurdi, H. Bertin, E. Martincic, M. De Kersauson, G. Fishman, S. Sauvage, A. Bosseboeuf, and P. Boucaud, Appl. Phys. Lett. **96**, 041909 (2010).

[60] J. Feng, X. Qian, C.-W. Huang, and J. Li, Nat. Photon. **6**, 866 (2012).

[61] G. H. Ahn, M. Amani, H. Rasool, D.-H. Lien, J. P. Mastandrea, J. W. Ager Iii, M. Dubey, D. C. Chrzan, A. M. Minor, and A. Javey, Nat. Commun. **8**, 608 (2017).

[62] S. Cahangirov, M. Topsakal, E. Aktürk, H. Şahin, and S. Ciraci, Phys. Rev. Lett. **102**, 236804 (2009).

[63] P. Jiang, X. Tao, H. Hao, L. Song, X. Zheng, L. Zhang, and Z. Zeng, 2D Mater. **4**, 035001 (2017).

[64] A. Fleurence, R. Friedlein, T. Ozaki, H. Kawai, Y. Wang, and Y. Yamada-Takamura, Phys. Rev. Lett. **108**, 245501 (2012).

[65] D. Chiappe, C. Grazianetti, G. Tallarida, M. Fanciulli, and A. Molle, Adv. Mater. **24**, 5088 (2012).

[66] B. Feng, Z. Ding, S. Meng, Y. Yao, X. He, P. Cheng, L. Chen, and K. Wu, Nano Lett. **12**, 3507 (2012).

[67] P. Vogt, P. De Padova, C. Quaresima, J. Avila, E. Frantzeskakis, M. C. Asensio, A. Resta, B. Ealet, and G. Le Lay, Phys. Rev. Lett. **108**, 155501 (2012).

[68] S. Cahangirov, V. O. Özçcelik, L. Xian, J. Avila, S. Cho, M. C. Asensio, S. Ciraci, and A. Rubio, Phys. Rev. B **90**, 035448 (2014).